CCFE
CULHAM CENTRE FOR FUSION ENERGY

UK Atomic Energy Authority

UKAEA-CCFE-PR(21)73

B. C. G. Reman, R. O. Dendy, T. Akiyama, M. Salewski, S. C. Chapman, J. W. S. Cook, H. Igami, S. Inagaki, K. Saito, R. Seki, G. S. Yun

Interpretation of transient bursts of ion cyclotron emission from fusion-born protons in deuterium plasmas in the Large Helical Device

Interpretation of transient bursts of ion cyclotron emission from fusion-born protons in deuterium plasmas in the Large Helical Device

B. C. G. Reman, R. O. Dendy, T. Akiyama, M. Salewski, S. C. Chapman, J. W. S. Cook, H. Igami, S. Inagaki, K. Saito, R. Seki, G. S. Yun

This is a preprint of a paper submitted for publication in Nuclear Fusion

Interpretation of transient bursts of ion cyclotron emission from fusion-born protons in deuterium plasmas in the Large Helical Device

B. C. G. Reman*[1], R. O. Dendy[2,1], T. Akiyama †[3], M. Salewski[4], S. C. Chapman[1], J. W. S. Cook[2,1], H. Igami[3], S. Inagaki[5], K. Saito[3], R. Seki[3], and G. S. Yun[6]

[1]Centre for Fusion, Space and Astrophysics, Department of Physics, Warwick University, Coventry CV4 7AL, UK

[2]CCFE, Culham Science Centre, Abingdon, Oxfordshire OX14 3DB, UK

[3]National Institute for Fusion Science, Toki, Gifu 509-5292, Japan

[4]Department of Physics, Technical University of Denmark, Fysikvej, Building 309, 2800 Kongens Lyngby, Denmark

[5]Research Institute for Applied Mechanics, Kyushu University, Kasuga 816-8580, Japan

[6]Department of Physics, Pohang University of Science and Technology, Pohang 37673, Korea

Abstract

During bursty MHD events, transient ion cyclotron emission (ICE) is observed from deuterium plasmas in the Large Helical Device (LHD) heliotron-stellarator. Unusually, the frequencies of the successive ICE spectral peaks are not close to integer multiples of the local cyclotron frequency of an energetic ion population in the likely emitting region. We show that this ICE is probably driven by a subset of the fusion-born protons near their birth energy $E_p = 3.02$MeV; this subset has a kinetic energy component parallel to the magnetic field, $m_p v_\parallel^2/2$, significantly greater than its perpendicular energy $m_p v_\perp^2/2$, for which $v_\perp \sim V_A$, the Alfvén speed. First principles computations of the collective relaxation of this proton population, within a majority thermal deuterium plasma, are carried out using a particle-in-cell approach. This captures the full gyro-orbit kinetics of all ions which, together with an electron fluid, evolve self-consistently with the electric and

*Now at Laboratoire Plasma et Conversion d'Energie, Université Paul-Sabatier Toulouse III, France

†Now at General Atomics, San Diego, CA, United States of America

magnetic fields under the Maxwell-Lorentz equations. We find substantial frequency shifts in the peaks of the simulated ICE spectra, and these correspond closely to the measured ICE spectra. The present study proposes that the transient ICE in LHD is generated by the identified subset of the fusion-born protons, relaxing under the magnetoacoustic cyclotron instability. So far as is known, this is the first report of a collective radiation signal from fusion-born ions in a non-tokamak magnetically confined plasma.

1 Introduction

The initial deuterium plasma campaign [1, 2, 3, 4, 5, 6, 7, 8] on the Large Helical Device (LHD) heliotron-stellarator has provided interesting new opportunities to study the fundamental physics of ion cyclotron emission (ICE) [9]. ICE was detected both during perpendicular deuterium neutral beam injection (NBI)[10] and during transient events. In this paper, we focus on the ICE that arises during transient events [11, 12, 13, 14, 15, 16, 17] which may be caused by the helically trapped energetic-ion-driven resistive interchange MHD mode (EIC), characterised by the mode numbers $m = 1$ and $n = 1$ (poloidal and toroidal respectively) [11, 12, 13, 14]. The abrupt onset of an associated tongue-shaped magnetic surface deformation has been reported in LHD [16, 17]. Contemporaneously, brief intense RF signals are detected in the hundreds of megahertz range, during which spectral peaks whose origin we address in this paper are found with a typical

spacing of 20MHz to 25MHz.

The much higher fusion reactivity of deuterium plasmas in LHD, compared to the negligible levels in previous hydrogen plasmas, generates fusion-born protons with energy $E_p = 3.02$ MeV. We propose here that a subset of these protons, with super-Alfvénic parallel velocities, are responsible for the transient ICE signal (shown, for example, in Fig. 1) that is observed during bursting events. This ICE signal is distinctive [18]: unusually, the frequencies of the successive spectral peaks are not close to integer multiples of the local cyclotron frequency of the energetic ion populations in the likely emitting region, whether fusion-born or neutral beam injected (NBI). We investigate how this ICE may be excited, and identify the likely physical origin of its distinctive frequency shift, by carrying out direct numerical simulations using a hybrid particle-in-cell (PIC) approach [19, 20, 21, 22]. Our computations follow the full gyro-orbit kinetics of hundreds of millions of ions, including both minority energetic ions (protons at 3.02 MeV) and majority thermal deuterons, together with an electron fluid, evolving self-consistently with the electric and magnetic fields under the Maxwell-Lorentz system of equations. The simulation domain spans one spatial axis and all three velocity coordinates (1D3V).

This PIC-hybrid approach was recently applied successfully to the interpretation of ICE from NBI protons in hydrogen plasmas in LHD [23]. In related work, the applicability of PIC computations for interpreting ICE from a subset of fusion-

born protons in deuterium plasmas was recently demonstrated for KSTAR observations [24, 25], and also for ICE driven by NBI deuterons in KSTAR deuterium plasmas [26]. In all these recent cases, as in the early ICE observations in JET [9] and TFTR [27] for example, the experimentally observed ICE spectral peaks are close to the cyclotron frequency of the energetic ions in the emitting region in the outer midplane plasma. In the corresponding PIC and PIC-hybrid computations [28, 21, 29, 22, 24, 25, 23], the minority energetic ion population is initialised with a physically motivated non-Maxwellian distribution in velocity space. This population then relaxes collectively under the magnetoacoustic cyclotron instability (MCI) [30, 31, 32], which in these simulations manifests at the level of the Maxwell-Lorentz dynamics of the individual particles and the self-consistent fields. The spatiotemporal Fourier transforms of the excited electric and magnetic fields that arise in the PIC-based computations then yield simulated ICE spectra, which compare well with observations.

Identification of the initial distribution in velocity space of the candidate ICE-generating energetic ion population, prior to relaxation under the MCI, is central to this approach. It typically rests on particle orbit studies, for example Fig. 14 of Ref. [9], Fig. 2 of Ref. [33], Fig. 2 of Ref. [24], Fig. 3 of Ref. [26] and Refs. [34, 35]. For the present application, we develop, as follows, our hypothesis for the velocity space distribution of the emitting sub-population of the protons recently born in deuterium fusion reactions with energy $E_p = 3.02$ MeV, which implies

that the emission location corresponds to the edge plasma. We first assume that, as usual, this ICE is dominated by waves propagating close to perpendicular to the local background magnetic field. Specifically, these waves are on the fast Alfvén-cyclotron harmonic wave branch; this follows from the analytical theory of the MCI [31], and is confirmed by analysis of the oscillations self-consistently excited in first principles PIC-based computations [28]. We assume that the ICE is primarily driven by a sub-population which can be characterised by a highly non-Maxwellian velocity space distribution, which we can model approximately in terms of a drifting-ring velocity distribution [36]

$$f\left(v_{\parallel}, v_{\perp}\right) = \frac{n_{energ.}}{2\pi v_{\perp}} \delta\left(v_{\perp} - v_{\perp,0}\right) \delta\left(v_{\parallel} - v_{\parallel,0}\right) \tag{1}$$

whose free parameters are its density $n_{energ.}$, $v_{\perp,0}$ and $v_{\parallel,0}$. On the basis of many previous studies of ICE and its driving instability, the MCI [37, 38, 39, 40, 41, 23], we fix $v_{\perp,0}$ to be close to the local Alfvén speed V_A, because this is a necessary condition for ICE to be strongly driven. We assume the driving ions are fusion-born protons at their birth energy $E_p = 3.02\text{MeV}$ because ICE unfolds on μs timescales during which no significant slowing-down occurs, such that their corresponding parallel component of kinetic energy is then

$$v_{\parallel,0}^2 = \frac{2}{m_p} E_p - v_{\perp,0}^2 \tag{2}$$

This defines a value for $v_{\|,0} > v_{\perp,0} \approx V_A$ which, when used in the PIC computations, gives rise to substantial spectral shifts in the simulated spectra. We shall show that these shifts correspond closely to the measured differences between ICE spectral peak frequencies and the integer harmonics of the local proton cyclotron frequency, that are observed during the transient events in LHD [11, 12, 16]. This tends to confirm our identification of the dominant ICE-generating energetic ion population as this particular subset of the fusion-born protons near their birth energy.

The present study is topical, in that recent observations from ASDEX-Upgrade [42] and DIII-D [43] exhibit increasing diversity and complexity in the distribution of ICE spectral peaks. There may be multiple candidate energetic ion species, both fusion-born and NBI, either sub- or super-Alfvénic, furthermore ICE is detected from the core plasma [44, 45], as well as from its traditional locus near the outer midplane edge [46, 43]. Frequency shifts of the kind examined here introduce a further degree of freedom to the frequency at which ICE spectral peaks are observed [37, 27, 33, 47, 48]. There is thus a new challenge, which one might term ICE plasma chemistry, in identifying the most likely ICE-generating ion species, together with their locations, from contemporary observed spectra where these are not immediately obvious. The localisation of the ICE-generating subset in velocity space, which follows from the present analysis of the LHD data presented in Figs. 1 and 2, provides an example of the reconstruction of the zeroth-order

features of the velocity space distribution function of an energetic ion population, based solely on ICE measurements [36, 49, 50, 51]. This in turn illustrates the diagnostic potential of ICE.

2 Observations of ICE during the transient event in LHD plasma 133979

The ICE acquisition system on LHD has been developed in partnership with KSTAR [52, 53, 54]. The measurement system comprises a dipole antenna located in the 10-O port of LHD, inside the vacuum vessel. A fast digitizer performs direct sampling of the radiofrequency measurements at a frequency of 1.25 GSamples/s. The time evolution of the RF signal intensity is collected by a 14-channel filter bank spectrometer in the range of 70MHz to 2800 MHz, with intermediate spectral resolution and with μs time resolution for a duration spanning the whole plasma discharge [54].

A distinctive ICE signal, in the frequency range between 200MHz and 300MHz, was detected during a transient event in LHD deuterium plasma 133979. This was heated with deuterium and hydrogen NBI: 59keV perpendicular and 170keV tangential, respectively. The measured perturbed magnetic field time series shown in Fig. 1 has spectral peaks (see also Fig. 2) whose separation could be related to the cyclotron frequency of an energetic ion species: in particular, the 3.02MeV

fusion-born protons, born in deuteron-deuteron fusion reactions. As we describe below, these spectra are different from ICE previously investigated. First the peaks appear to have undergone substantial Doppler shifts with respect to local integer cyclotron harmonics; and second, the frequency interval between successive peaks is not strictly uniform. As an example of this ICE phenomenology, the top left panel of Fig. 1 shows the time series of the magnetic field intensity of the bursting ICE at $t \approx 4.443$s in LHD plasma 133979, and the top right panel shows the corresponding spectrogram displaying intense radio frequency activity in the hundreds of megahertz range. This spectrogram is plotted with increasingly high time resolution in the two bottom panels of Fig. 2. We shall show that these effects can arise naturally from the substantial super-Alfvénic parallel velocity of the energetic protons that, we argue, drive this ICE.

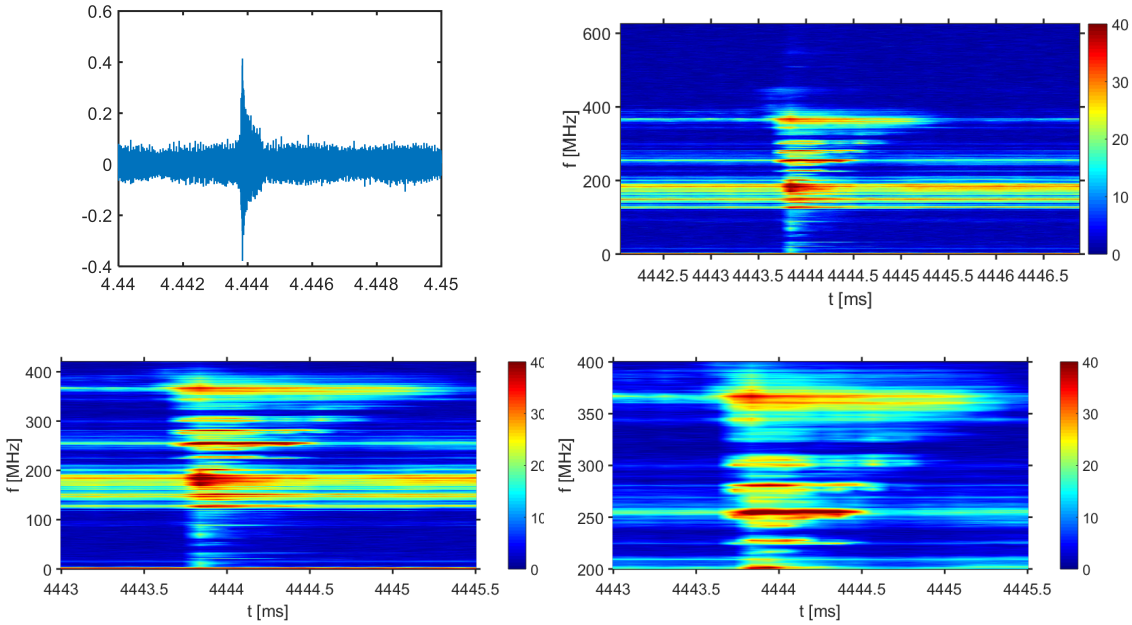

Figure 1: ICE phenomenology measured during the bursty MHD event in LHD plasma 133979. (Top left) Time series of the magnetic field fluctuations (au). (Top right) Corresponding windowed Fourier transform showing the time evolution of the frequency content in the hundreds of MHz range. (Bottom panels) The ICE feature plotted at higher time resolution across narrower frequency domains.

Figure 2 presents two ICE power spectra, taken (top) just before the bursty event at $t = 4.440$s, and (bottom) during the event at $t = 4.444$s. The major difference consists in the appearance during the burst of the three peaks labelled b, c, d in the lower panel, together with peak a. The average of the slightly unequal frequency separations between these peaks b, c and d is $\Delta f = 26.6$MHz. Figure 3 displays the time evolution of the measured neutron flux between $t = 3.0$s and $t = 5.5$s during LHD plasma 133979. This signal reaches its maximum value

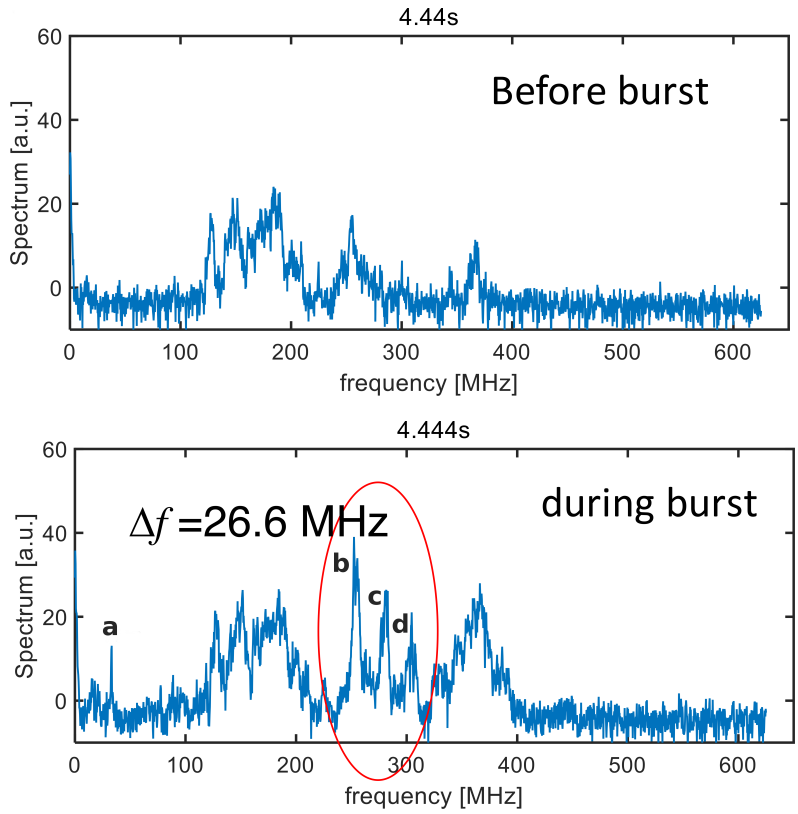

Figure 2: ICE power spectra from LHD plasma 133979 before (top panel) and during (bottom) the bursty MHD event. The spectrum at the time of the bursty event exhibits three intense peaks b, c and d, together with peak a, and there is additional activity above 300MHz. The peaks b, c and d are at 255.1MHz, 281.7MHz and 308.2 MHz; peak a is at 32.73MHz.

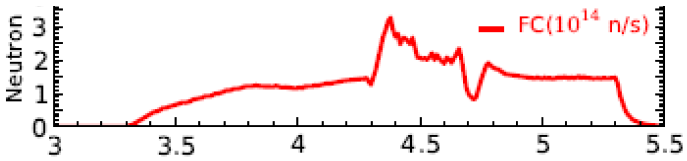

Figure 3: Measured neutron flux from LHD plasma 133979 plotted versus time (in seconds). The signal reaches peak amplitude at $t \sim 4.43$s, slightly before the bursty event occurs.

at $t \sim 4.43$s shortly before the bursty event, and decreases following it; there is probably a causal link [6] which results in an inversion in the velocity space of the fusion-born protons capable of driving ICE. The top panel of Fig. 4 shows that the NBI power is steady around the time of the burst, between 4.4s and 4.6s. The middle and bottom panels plot the time evolution of the power radiated by the plasma in six different radio frequency channels, between 100MHz and 800MHz. Intense transient activity is visible. The origin of the activity at the highest frequencies, 600MHz and 880MHz in the bottom panel, is not clear. In the present paper, we focus on the energetic ion physics underlying the radio frequency bursts in the range 200MHz to 300MHz.

13

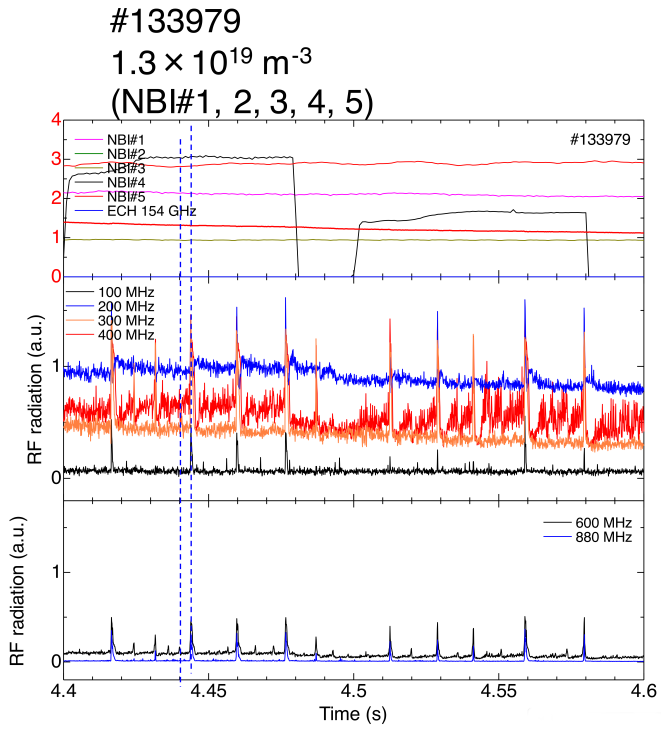

Figure 4: (Top) Time evolution of NBI power and (lower two panels) radio frequency intensity emitted from the plasma across six frequency channels. The two blue vertical dashed lines indicate the times just before the burst at $t = 4.440$s, and during the burst at $t = 4.444$s, that correspond to the ICE spectra in Fig. 2.

3 Identification of the candidate sub-population fusion-born protons

The redistribution of the initially helically-trapped ions that are implicated in burst kinetic MHD [11, 12, 14] or abrupt tongue deformation [16, 17] could generate a distinct, transient, highly non-Maxwellian distribution in velocity space, perhaps involving the expelled ions and freshly trapped ions. Let us therefore make the assumption (for this, or some as-yet-unknown, reason) that a transient, spatially localised, highly non-Maxwellian population of 3.02MeV fusion-born protons could be responsible for the ICE spectral peaks b, c and d in Fig. 2. Our initial goal is then to perform multiple PIC-hybrid computations of the collective relaxation of these highly energetic protons, using the plasma parameters at an appropriately inferred ICE emission location; and to investigate whether the resulting simulated ICE power spectra are compatible with the measurements in Fig. 2. In this section, we identify the fundamental cyclotron frequency with the mean frequency spacing between the peaks b, c and d. This allows us to determine the emission location and thus the plasma parameters necessary to initialise our simulations in section 4. Alternatively in section 5, peak a defines the fundamental cyclotron frequency from which steps of section 4 are repeated. These approaches share the assumption that these peaks have a common emisson location. If the radiation is generated by protons, identifying the 26.6MHz mean frequency spacing

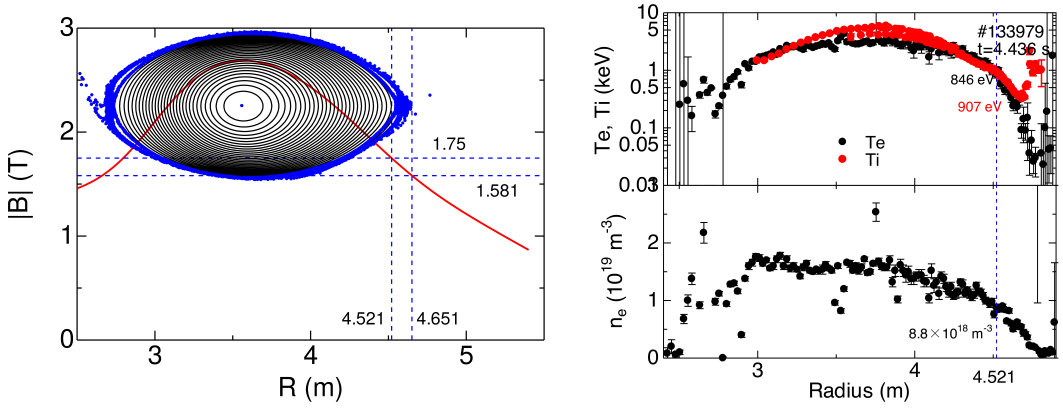

Figure 5: (Left) Profile of magnetic field strength as a function of major radius in LHD, overplotted on a poloidal cut of magnetic surfaces. (Right) Radial profile of electron and ion temperature (upper) and electron number density (lower), around the burst occurrence time $t \approx 4.43$s. In the poloidal cross section which has horizontal elongation, magnetic field strength 1.75T corresponds to $R = 4.521$m.

between these peaks as an indicative local proton cyclotron frequency implies a local magnetic field strength of 1.75T, see Fig. 5. The corresponding radius in LHD magnetic geometry is 4.521m, which is close to the last closed magnetic surface. The electron and deuterium temperatures at this estimated emission location are 846eV and 907eV respectively, while the electron number density is 8.8x10^{18}m^{-3}; these are used as input parameters in our PIC-hybrid simulations.

The table [35] displayed as Fig. 6 gives the computed time after which 3.02MeV protons are lost, as a function of their radial birth location and of their initial pitch angle, evaluated in the equatorial plane of LHD. The red boxes are the initial locations corresponding to unconfined fusion-born protons. Conversely, there

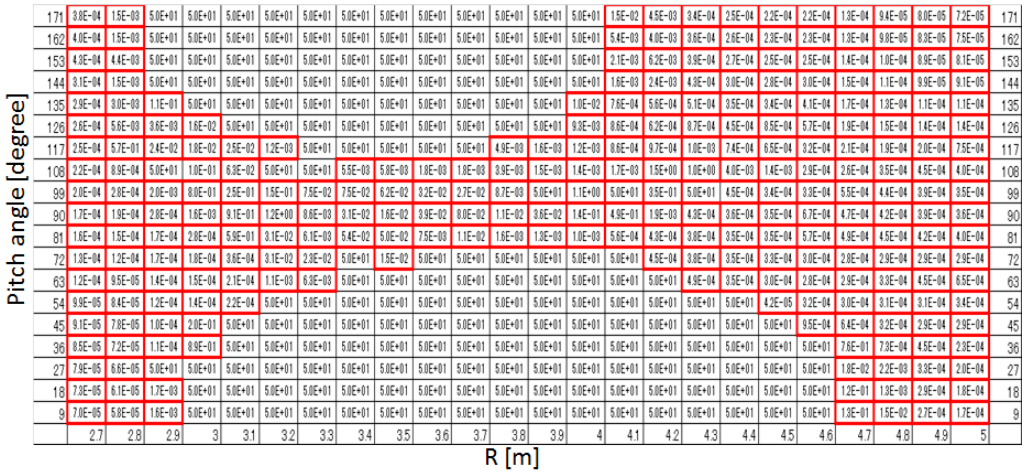

Figure 6: Table from Ref. [35] showing the time after which a 3.02 MeV proton born in LHD is lost as a function of major radial location and pitch angle (defined by Eq. 6) at birth, evaluated on the equatorial plane of LHD. Each number in this table is the time before loss, in milliseconds. Red boxes denote promptly lost protons. The remaining protons constitute the local confined population and define its velocity distribution. The underlying calculation [35] tracks the guiding centre, and collisions are neglected because their timescale is long compared to the timescales on which ICE unfolds.

is the possibility for fusion-born protons to remain on confined trajectories [55]. Further studies have shown that other particles in the MeV energy range can be confined in LHD [55], for example some 15MeV protons resulting from the D + ^{3}He $\rightarrow$ ^{4}He (3.67 MeV) + p (15 MeV) reaction are confined over the chaotic field line region [56]. In order to make use of the information in Fig. 6 to establish whether the candidate ICE-generating protons at the location of the ICE bursts are indeed confined, we need to establish a mapping between particle velocity vectors there and at the birth location. We first calculate the magnetic moment

of the potentially confined sub-population of 3.02MeV fusion-born protons at the burst location, which we denote by

$$\mu_{ICE} = \frac{m_H v_{\perp,burst}^2}{2B_{burst}} \tag{3}$$

Here the value of $v_{\perp,burst}$, which denotes the perpendicular velocity of the ICE-emitting ions at the burst location, is not exactly known but is strongly constrained, as we describe below; and we assume $B_{burst} = B_{ICE} = 1.75$T, as already established. We now invoke the conservation of magnetic moment $\mu_{ICE} = \mu_R$, with $\mu_R = m_H v_{\perp,R}/2B_R$ the magnetic moment at major radius R, where the local perpendicular velocities of the protons is denoted by $v_{\perp,R}$, and the corresponding local magnetic field is denoted B_R. It follows that

$$v_{\perp,R} = \sqrt{\frac{2B_R\mu_{ICE}}{m_H}} \tag{4}$$

Equating the total kinetic energy, which is the sum of perpendicular and parallel components, to the birth energy, we have

$$\frac{1}{2}m_H v_R^2 = \frac{1}{2}m_H v_{\perp,R}^2 + \frac{1}{2}m_H v_{\parallel,R}^2 = 3.02\text{MeV} \tag{5}$$

We can then compute the pitch angles α at the inferred birth locations,

$$\alpha = \arcsin\left(\frac{v_{\perp,R}}{v_R}\right) \tag{6}$$

for $v_{\perp,burst} = [0.8, 0.9, 1.0, 1.1, 1.2]\, V_A$ at $R = 4.521$m. This range of values for $v_{\perp,burst}/V_A$ is chosen because it is known to give strong drive for the MCI and hence ICE [28]. Finally, we compare these values with those tabulated in Fig. 6, to find out whether these protons are born on confined trajectories. The values of α are displayed in Table 1, and suggest that the protons that intersect the burst location in the range of velocities considered were originally born on confined trajectories, as identified for LHD in Fig. 6.

R (m)	3.10	3.20	3.30	3.40	3.50	3.60	3.70	3.80	3.90	4.00	4.10	4.20	4.30	4.40	4.50	4.60
B_R (T)	2.28	2.42	2.56	2.64	2.68	2.69	2.66	2.61	2.53	2.43	2.33	2.20	2.06	1.92	1.78	1.65
$0.8V_A$	20.29	20.94	21.56	21.91	22.08	22.13	21.98	21.78	21.42	20.99	20.52	19.91	19.23	18.55	17.83	17.14
$0.9V_A$	22.96	23.71	24.42	24.82	25.01	25.07	24.91	24.68	24.26	23.76	23.22	22.53	21.75	20.97	20.15	19.36
$1.0V_A$	25.69	26.54	27.35	27.80	28.02	28.09	27.90	27.64	27.17	26.59	25.98	25.19	24.31	23.44	22.51	21.61
$1.1V_A$	28.48	29.44	30.35	30.87	31.12	31.19	30.98	30.68	30.15	29.50	28.81	27.92	26.93	25.94	24.90	23.90
$1.2V_A$	31.34	32.42	33.45	34.04	34.32	34.40	34.16	33.83	33.22	32.49	31.72	30.72	29.60	28.51	27.35	26.23

Table 1: Birth pitch angles α, defined by Eq. 6, expressed in degrees at different major radial locations R, which for a 3.02 MeV proton lead to perpendicular velocities of $v_{\perp,burst} = (0.8, 0.9, 1.0, 1.1, 1.2)V_A$ at R=4.521m. It follows that these protons lie in the confined region of (α, R) parameter space delineated by the lower black region in Fig. 6 since the pitch angles calculated here do not exceed 35°. These pitch angle values are therefore smaller than those which lead to promptly lost ions indicated in Fig. 6 for the range $R = 3.10$m to $R = 4.60$m.

The foregoing suggests that 3.02MeV protons with perpendicular velocities in the range $v_{\perp,burst} = [0.8-1.2]V_A$ at the location of interest are on confined trajectories. In the next section, we will show that they could efficiently drive the observed transient ICE signal. In contrast, the velocities of the energetic deuterons from perpendicular NBI are very sub-Alfvénic at the ICE location. Typically, these have $v_\perp/V_A < 0.3$, so that their ability to drive the MCI would be weak [23, 25], and we need not consider them further here.

4 Simulations of bursting ICE from LHD plasma 133979

4.1 Frequency shifts and energy partitioning

The three intense peaks *b*, *c* and *d* in Fig. 2 are at frequencies 255.1, 287.1 and 308.2 MHz. In the preceding section, we used the average spacing between neighbouring peaks, 26.6MHz, as an interim value for the proton cyclotron frequency Ω_H at the ICE location. If we normalize the three spectral peak frequencies to 26.6MHz, they would correspond to proton cyclotron harmonics 9.6, 10.6 and 11.6, which are evidently not integer multiples of the fundamental. To progress, we first evaluate the frequency differences between the measured spectral peaks and the

nearest sequence of integer harmonics of Ω_H, which could be either $(9, 10, 11)$ or $(10, 11, 12)$. If we evaluate $[308.2, 281.7, 255.1]$ MHz $-26.6 \times [11, 10, 9]$ MHz, we obtain positive shifts that equate to $[15.6, 15.6, 15.7]$ MHz, or 0.6×26.6MHz. The shifts are negative with respect to harmonics 10, 11 and 12: $[308.2, 281.7, 255.1]$ MHz $-26.6 \times [12, 11, 10]$ MHz $= [-11.0, -10.90, -10.90]$MHz, or -0.4×26.6 MHz. In either case, then, the measured frequency shifts relative to integer cyclotron harmonics have magnitude $\simeq \Omega_H/2$.

Let us first examine whether, in principle, in the present context, it is plausible that there could arise Doppler shifts of 15.7MHz (harmonics 9,10,11) or -10.9MHz (harmonics 10,11,12). It is well known [57, 28, 21] that to excite the MCI requires the energetic ions to have perpendicular velocity $v_\perp \approx V_A$. If the total kinetic energy of the ions is sufficiently large that this value of $v_\perp$ is compatible with $v_\parallel \simeq V_A$ also, this would provide scope for Doppler shifts satisfying $k_\parallel v_\parallel \sim \Omega_H$ if $k_\parallel V_A \sim \Omega_H$. This is equivalent to $\left(k_\parallel/k_\perp\right) k_\perp V_A \sim \Omega_H$. In the MCI, a quasi-perpendicular fast Alfvén wave is resonant with the nth proton cyclotron harmonic: $\omega_{fast} \simeq k_\perp V_A \simeq n\Omega_H$. The MCI is typically [9] most strongly driven around the tenth proton cyclotron harmonic in deuterium plasmas, i.e. $n = 10$, see Fig. 1 of Refs. [28, 21] and Fig. 4 of Ref. [25]. For sufficiently energetic ions undergoing the MCI, this suggests it is therefore possible to satisfy $k_\parallel v_\parallel \sim \Omega_H$ at $\omega \sim n\Omega_H$ if $k_\parallel/k_\perp \sim 1/n$. It follows - but only at back-of-envelope level - that it might be possible for a strongly non-Maxwellian population of 3.02MeV protons

to excite, through the MCI, waves at cyclotron harmonics that are Doppler shifted by the large amount $\sim \Omega_H/2$ that is observed. As an illustration, let us suppose

$$\left|k_\parallel v_\parallel\right| \sim \Omega_H/2 \tag{7}$$

for waves excited on the fast Alfvén branch at the tenth harmonic of Ω_H, so that

$$\omega \sim k_\perp V_A \sim 10\Omega_H \tag{8}$$

Then upon taking the ratio of each side of Eqs. 7 and 8, we find

$$\frac{k_\parallel}{k_\perp} \sim \frac{V_A}{20u_\parallel} \sim \frac{1}{48.4} \tag{9}$$

for the case $u_\parallel = 2.42V_A$ which is inferred from Eq. 10 of Section 4.3 when $u_\perp = 1.05V_A$. It follows that fast Alfvén waves propagating only 1° or 2° from perpendicular to $\mathbf{B}_0$ could in principle undergo wave-particle cyclotron harmonic resonance at the required, highly shifted, frequency of approximately $10\Omega_H \pm \Omega_H/2$. The question then is: are such waves actually excited? This motivates our direct numerical simulations reported below.

Table 2 displays the consequences of different partitions of the 3.02MeV proton birth energy into perpendicular and parallel components, in terms of the corresponding perpendicular and parallel velocities normalised to the local Alfvén

Species	$v_\perp/V_A$	Energy $\perp$ (keV)	$v_\parallel/V_A$	Energy $\parallel$ (keV)	ω_{Drift}/Ω_H
H	0.50	108.16	2.59	2891.84	0.0144
H	0.60	155.76	2.56	2844.24	0.0143
H	0.63	170.00	2.63	2830.00	0.0142
H	0.70	212.00	2.54	2788.00	0.0141
H	0.80	276.90	2.51	2723.10	0.0140
H	0.90	350.45	2.47	2649.55	0.0138
H	1.00	432.66	2.44	2567.34	0.0136
H	1.10	523.52	2.39	2476.48	0.0134
H	1.20	623.03	2.34	2.376.97	0.0131

Table 2: The consequences of different partitions of 3.02MeV proton energy into perpendicular and parallel components, expressed in terms of velocities normalised to the local Alfvén speed in the ICE emitting region of LHD plasma 133979 during the bursty event at $t = 4.444$sec. The last column shows the corresponding circulation frequency due to the combined curvature and grad B guiding centre drifts, and demonstrates that this is small compared to Ω_H.

speed at the emission location in LHD. In addition, the last column shows that the Doppler shift due to the combined curvature and grad B drift [58] is an order of magnitude smaller than the frequency shift inferred from the measured power spectrum in Fig. 2. We shall use PIC-hybrid simulations to explore the range of $k_\parallel$ which, together with $v_\parallel$, could result in frequency shifts consistent with the measured ICE power spectrum. Hitherto, no wavenumber measurements of ICE have been reported from LHD. Each PIC-hybrid computation is run at a given angle between the magnetic field $\mathbf{B}_0$ and the 1D spatial simulation domain, which we identify as the outward radial direction in LHD, and which defines the

orientation of possible **k** vectors.

4.2 Simulations with zero parallel velocity

As a first step in isolating the role of $v_\parallel$, we run simulations for which $v_\parallel = 0$, so that the initial velocity distribution function of protons is given by a ring beam $f_H = n_{proton}/\left(2\pi v_\perp\right)\delta\left(v_\parallel\right)\delta\left(v_\perp - u_\perp\right)$. This enables us to focus on the role of $u_\perp$. We know that $u_\perp \approx V_A$ is necessary for the MCI to occur. With $u_\perp$ in this range, and $u_\parallel = 0$ for now, the total kinetic energy of such protons is less than 3.02MeV. We explore a range of perpendicuar velocities from $u_\perp = 0.8V_A$ to $1.2V_A$. These computations use 500 particles per cell for the thermal deuterons and for the fast protons, and represent the electrons as a massless fluid. The grid has 1024 cells, and the cell size is chosen such that the cold plasma dispersion relation is recovered from the spatiotemporal Fourier transform of the electric and magnetic field fluctuations, in the appropriate limit. The time evolution of the fields and of the ion species energy density from our PIC-hybrid simulations show that the collective relaxation of the 3.02MeV proton population is governed by the MCI, as seen in Fig. 7. It is known that the MCI drive scales with the relative number density $\xi = n_{proton}/n_e$ in the relevant regime [22]. In the simulations described below, the value of ξ is chosen to saturate the MCI within $20\tau_D$: $\xi = 0.0025$ for orientation of the spatial domain with respect to $\mathbf{B}_0$ of 90.5°, 91.0° and 91.5°; and $\xi = 0.0050$ for 92.0°. This approach optimises the use of computational re-

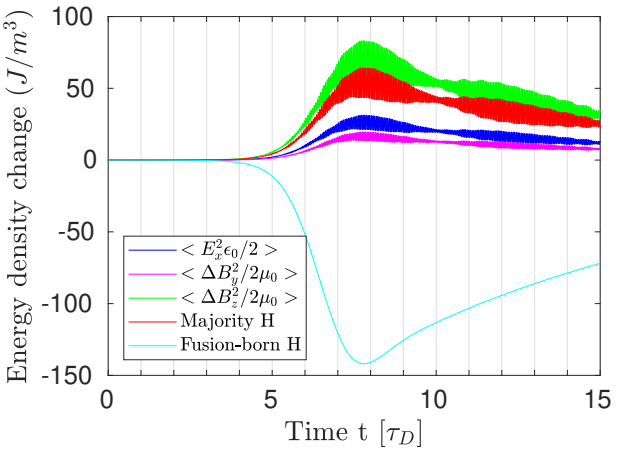

Figure 7: Time evolution of the energy density change of the fields and of the thermal deuterons and fusion-born proton population. The latter collectively relaxes under the MCI and cedes its energy to excite the electric and magnetic fields, and cause the thermal deuterons to oscillate self-consistently. The magenta and green traces correspond to the y and z-component of the magnetic field. The blue and red curves show the energy density change of the x-component of the electric field and of the thermal deuterons respectively. The propagation angle between the simulation domain and the background magnetic field $\mathbf{B}_0$ is 91°. The time is normalised to the deuteron gyroperiod τ_D.

sources (each simulation requires two hours on 56 cores) without compromising the physics.

The resulting power spectra shown in Fig. 8 are for a range of values of the perpendicular component of velocity $0.8 \leq u_\perp/V_A \leq 1.2$. The spectral peaks are at successive proton cyclotron harmonics, and in this respect they differ, as expected, from the LHD ICE observations in Fig. 2 that we seek to explain. These preliminary simulation results are encouraging in relation to the essential feature of the ICE spectrum in Fig. 2, measured during the LHD transient, in that the simulated spectra are dominated by a few cyclotron harmonic peaks in the frequency range between $\omega = 8\Omega_H$ and $12\Omega_H$.

The magnitude of the most strongly driven spectral peaks in Fig. 8 tends to decrease monotonically as $u_\perp$ increases, and this feature is most notable when the propagation angle gets closer to 90°. Figure 9 shows the sensitivity of the spectral peak maxima to the propagation angle, as well as to the perpendicular beam velocity in the range $0.925 \leq u_\perp/V_A \leq 1.050$. It confirms that, in these initial computations for the restricted case $u_\parallel = 0$, the MCI of a ring-beam population of energetic protons with $u_\perp \sim V_A$ generates simulated ICE spectra whose dominant peaks are in the observationally significant range between $9\Omega_H$ and $12\Omega_H$. We have found that this spectral range is also dominant for an initial fast proton distribution which incorporates perpendicular thermal spread [36] $f_H \propto \exp\left[-\left(v_\perp - u_\perp\right)^2/v_{\perp,r}^2\right]$ with $v_{\perp,r} = 0.15u_\perp$.

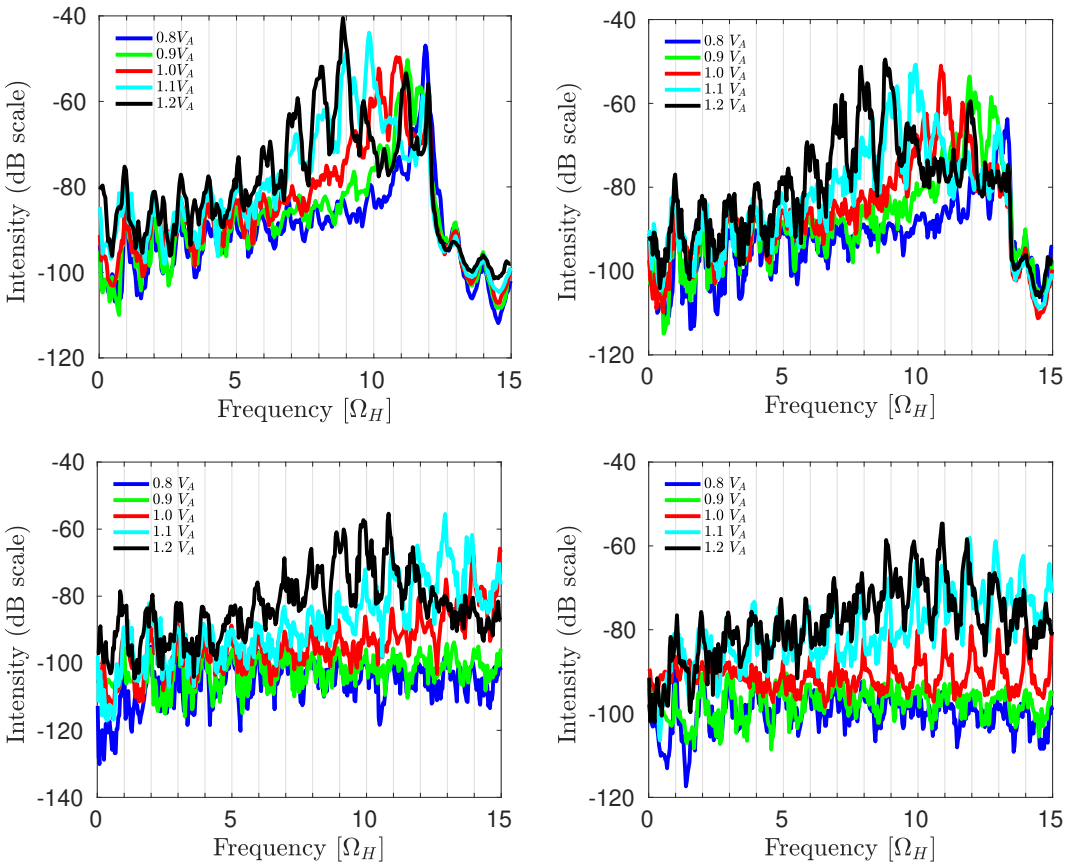

Figure 8: Power spectra of the excited δB_z energy density in multiple computations of the relaxation of a ring-beam ($v_\parallel = 0$) distribution of protons for LHD plasma 133979 parameters at the time and location of the bursting ICE event. For the five spectra plotted in each panel, the protons have purely perpendicular velocity $u_\perp$: from top, $u_\perp = 1.2V_A$, $1.1V_A$, $1.0V_A$, $0.9V_A$ and $0.8V_A$. The propagation angle between $\mathbf{k}$ and $\mathbf{B}_0$ is 90.5° (top left), 91.0° (top right), 91.5° (bottom left), 92.0° (bottom right).

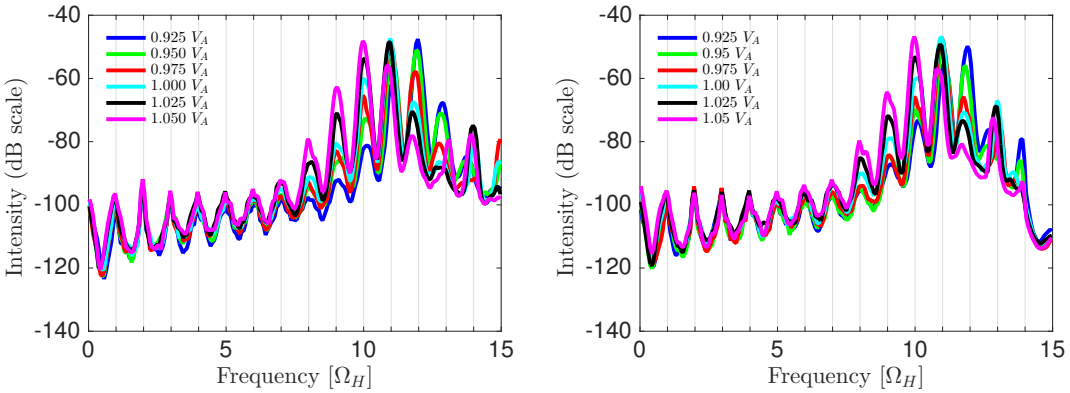

Figure 9: Power spectra for oscillations excited by a ring-beam ($v_\parallel = 0$ proton population) at a propagation angle of 91.0° (left), and 90.8° (right), for different perpendicular beam velocities (inset), in the range $0.925 \leq u_\perp/V_A \leq 1.050$. In both cases, the four dominant spectral peaks that result from the simulations are the ninth to twelfth harmonics of Ω_H. These correspond exactly to the four cyclotron harmonics of greatest relevance to the interpretation of the measured ICE spectral peaks *b*, *c* and *d* in Fig. 2.

4.3 Simulations with realistic parallel velocity

The simulation results obtained in the preceding sub-section 4.2, for the case where the driving proton population has no velocity component parallel to the magnetic field, indicate that the range of angles and $u_\perp/V_A$ values considered give rise to healthy, and potentially experimentally relevant, MCI-driven power spectra. Let us now focus in particular on $u_\perp/V_A = 1.05$, and introduce parallel velocities into our approach. For fusion-born protons, the initial kinetic energy $E = \left(u_\perp^2 + u_\parallel^2\right)/2m_H = 3.02\text{MeV}$. Since

$$u_\parallel = \left[2E/m_H - (u_\perp)^2\right]^{1/2} \tag{10}$$

it follows that if $u_\perp = 1.05V_A$, then $u_\parallel = 2.42V_A$ for a 3.02MeV proton. In the series of PIC-hybrid computations described in this sub-section, we use these values for $u_\perp$ and $u_\parallel$ (together with other pairings derived in the same way; see Table 2) as parameters in the simple model distribution function of the fusion-born protons

$$f_H\left(v_\perp, v_\parallel\right) = \frac{n_H}{2\pi v_\perp}\delta(v_\parallel - u_\parallel)\delta(v_\perp - u_\perp) \tag{11}$$

We have run PIC-hybrid simulations for minority 3.02MeV proton populations, initialised using Eqs. 10 and 11, in majority thermal deuterium plasmas. We use 2000 particles per cell for each ion species, with 8192 cells, and a duration of $15\tau_D$. Power spectra are constructed from the spatiotemporal Fourier transform

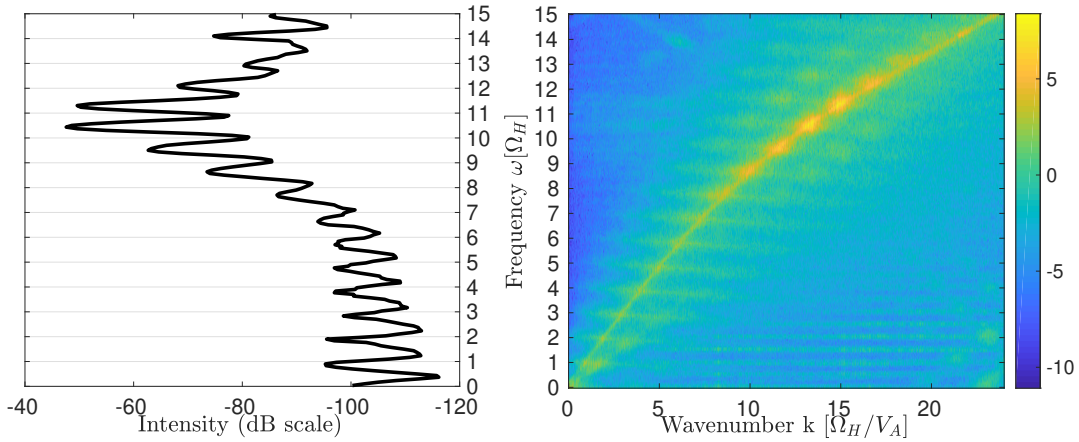

Figure 10: The power spectrum of δB_z (left) is constructed from the spatiotemporal Fourier transform of δB_z (right). These are plotted on a dB and $\log_{10}$ scale respectively, for the fields excited by the relaxation of a 3.02MeV proton population initialized with $n_H/(2\pi v_\perp)\delta(v_\parallel - u_\parallel)\delta(v_\perp - u_\perp)$, $u_\perp = 1.05V_A$ and $u_\parallel = 2.42V_A$. The propagation angle between $\mathbf{k}$ and $\mathbf{B}_0$ is 91.0°, and the majority thermal ions are deuterons.

of δB_z, taken over the full spatial domain and averaged over $15\tau_D$. This is shown on the right panel of Fig. 10, where the fast Alfvén branch and multiple cyclotron harmonic wave branches are clearly visible. Summing the Fourier transformed power between $k = 0$ and $k = 24\Omega_H/V_A$ yields the power spectrum shown on the left panel in Fig. 10. This is identical to the green trace shown in Fig. 11 (left). Figure 11 shows the power spectra of waves propagating in the $+\hat{\mathbf{x}}$ direction (corresponding to the direction of the 1D simulation domain) at an angle of 91.0° and 90.8° with respect to the background magnetic field $\mathbf{B}_0$. The green power spectra result from 3.02MeV protons whose parallel and perpendicular velocities

are $u_{\parallel} = 2.415 V_A = 2.199 \times 10^7 \mathrm{ms}^{-1}$ and $u_{\perp} = 1.050 V_A = 0.956 \times 10^7 \mathrm{ms}^{-1}$; while the blue traces have the same value of $u_{\perp}$ but with $u_{\parallel} = 0$, for comparison (as in sub-section 4.2). The frequency resolution in the computed spectra is $\pm 0.07 \Omega_H$. In the blue cases, for zero $u_{\parallel}$, three intense spectral peaks appear at $9\Omega_H$, $10\Omega_H$ and $11\Omega_H$. For the green traces in Fig. 11, with $u_{\parallel} = 2.42 V_A$, the dominant spectral peaks are at: $9.50\Omega_H$, $10.44\Omega_H$ and $11.30\Omega_H$ for 91.0° propagation angle; and at $9.57\Omega_H$, $10.50\Omega_H$ and $11.30\Omega_H$ for 90.8°. We note immediately that the spectral peak frequencies are shifted by approximately $\Omega_H/2$, similar to the observational shifts noted at the start of sub-section 4.1

For a second set of simulations using protons initialised with $u_{\perp} = 0.950 V_A = 0.865 \times 10^7 \mathrm{ms}^{-1}$ and $u_{\parallel} = 2.470 V_A = 2.244 \times 10^7 \mathrm{ms}^{-1}$, at a propagation angle of 89.0°, the MCI-excited spectrum is shown in Fig. 12. This has major peaks at $9.49\Omega_H$, $10.57\Omega_H$ and $11.57\Omega_H$.

As noted at the start of sub-section 4.1, the observed frequencies of the ICE spectral peaks b, c and d in Fig. 2 could be provisionally identified with $9.6\Omega_H$, $10.6\Omega_H$ and $11.6\Omega_H$. The extent of agreement between these experimental values and the results of first principles simulation embodied in the green spectra of Figs. 11 and 12 appears encouraging. The four dominant spectral peaks as a function of $\left(u_{\perp}, u_{\parallel}\right)$ are given in Tables 3 and 4 for waves propagating in the $+\hat{\mathbf{x}}$ direction of the simulation domain, at angles of 91.0° and 89.0° with respect to the background magnetic field $\mathbf{B}_0$.

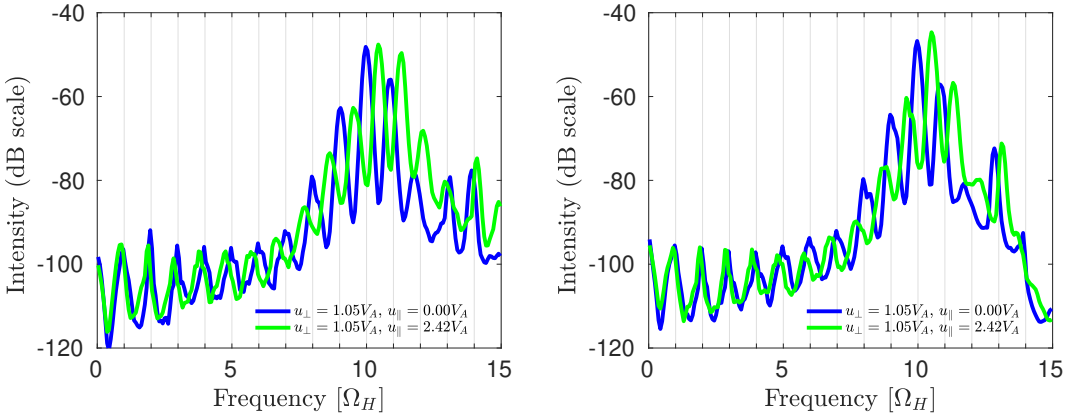

Figure 11: Power spectra of δB_z from PIC-hybrid computations with the orientation of the spatial domain $\hat{\mathbf{x}}$ at an angle of 91.0° (left) and 90.8° (right) with respect to the background magnetic field. Only excited waves propagating in the $+\hat{\mathbf{x}}$ direction are included. The initial energetic proton distribution functions are $n_H/(2\pi v_\perp)\delta(v_\parallel)\delta(v_\perp - u_\perp)$ (blue trace) and $1/(2\pi u_\perp)\delta(v_\parallel - u_\parallel)\delta(v_\perp - u_\perp)$ (green trace). The velocities are $u_\parallel = 2.199 \times 10^7 \mathrm{ms}^{-1}$ and $u_\perp = 0.956 \times 10^7 \mathrm{ms}^{-1}$, corresponding to $u_\perp = 1.05V_A$ and $u_\parallel = 2.42V_A$ and are such that $m_H(u_\parallel^2 + u_\perp^2)/2 = 3.02\mathrm{MeV}$. The dominant spectral peaks for the green traces are at: (left) $9.50\Omega_H$, $10.44\Omega_H$ and $11.30\Omega_H$; (right) $9.57\Omega_H$, $10.50\Omega_H$ and $11.30\Omega_H$.

$u_\perp$, $u_\parallel$ (V_A) \ ℓ	9	10	11	12	13	14	15
$u_\perp = 0.90$, $u_\parallel = 2.48$	-	-	-	11.37	12.30	13.10	13.97
$u_\perp = 0.95$, $u_\parallel = 2.47$	-	-	10.44	11.37	12.24	13.04	-
$u_\perp = 1.00$, $u_\parallel = 2.44$	-	9.57	10.44	11.30	12.17	-	-
$u_\perp = 1.05$, $u_\parallel = 2.42$	-	9.50	10.44	11.30	12.10	-	
$u_\perp = 1.10$, $u_\parallel = 2.39$	8.70	9.57	10.37	11.17	-	-	

Table 3: Location of the four major peaks in the simulated ICE spectrum, in units of Ω_H, for drifting ring-beam populations of minority 3.02 MeV protons initialised with five different combinations of $(u_\perp, u_\parallel)$ as shown. In all cases the waves are forward propagating, and the propagation angle between the simulation domain and the background magnetic field $\mathbf{B}_0$ is 91.0°. The frequency resolution in the computed spectra is $\pm 0.07\Omega_H$.

There is a further potentially significant aspect to the simulated power spectra shown by green traces in Figs. 11 and 12, which correspond to simulations with super-Alfvénic $u_\parallel$: the peaks at lower frequencies lie very close to low integer cyclotron harmonics. This is in contrast to the substantial frequency shifts that are visible at higher harmonics, and are tabulated in Tables 3 and 4. The absence of a shift for the lowest frequency spectral peaks in our simulations suggests that, in the measured LHD ICE spectrum of Fig. 2, the spectral peak a at the lowest frequency may define the proton cyclotron frequency at the location from which the ICE originates. We shall exploit this and explain it in section 5.

$u_\perp$, $u_\parallel$ (V_A) \ ℓ	7	8	9	10	11	12	13
$u_\perp = 0.90$, $u_\parallel = 2.48$	-	-	-	10.57	11.64	12.64	13.7
$u_\perp = 0.95$, $u_\parallel = 2.47$	-	-	9.50	10.57	11.57	12.57	-
$u_\perp = 1.00$, $u_\parallel = 2.44$	-	8.44	9.50	10.50	11.50	-	-
$u_\perp = 1.05$, $u_\parallel = 2.42$	7.30	8.37	9.44	10.37	-	-	-
$u_\perp = 1.10$, $u_\parallel = 2.39$	7.30	8.37	9.44	10.37	-	-	-

Table 4: The same as Table 3 for a propagation angle of 89°.

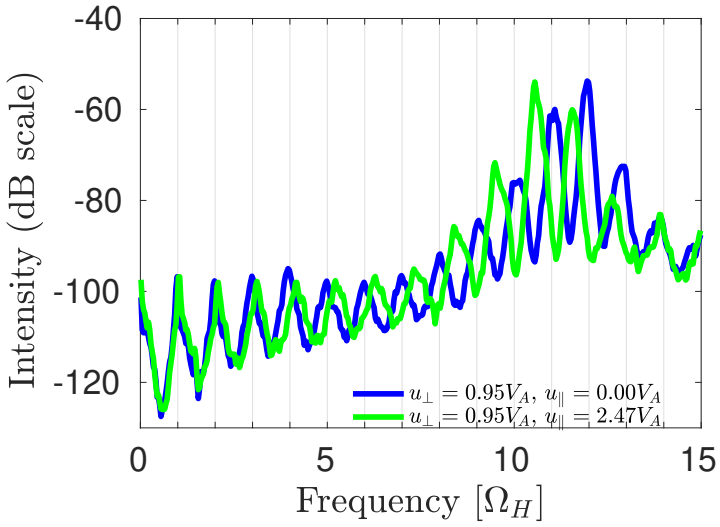

Figure 12: Power spectrum of δB_z from a PIC-hybrid computation for waves excited propagating in the $+\hat{\mathbf{x}}$ direction, which is oriented at an angle of 89.0° with respect to the background magnetic field. The initial energetic proton distribution functions have the form defined in the caption to Fig. 11, with $u_\perp = 0.95V_A$ and $u_\parallel = 2.47V_A$. The dominant spectral peaks for the green traces are at $9.49\Omega_H$, $10.57\Omega_H$ and $11.57\Omega_H$.

5 Simulations using the lowest ICE spectral peak as a point of reference

Thus far, we have focused on the three peaks between 250 and 310MHz in the observed transient ICE power spectrum, Fig. 2, during LHD deuterium plasma 133979. The simulated ICE spectra that also result from our first principles PIC-hybrid computations, shown in Figs. 11 to 12, strongly suggest that these three observed ICE spectral peaks arise from MCI physics in the frequency range between about seven and eleven proton cyclotron harmonics. These three peaks are strongly shifted with respect to integer multiples of Ω_H in our simulations corresponding to the green traces in Figs. 11 and 12, and this feature quantitatively reinforces the link to the ICE observations. At the fundamental of Ω_H, however, the green traces exhibit no significant frequency shift. This motivates the hypothesis that, in the observed ICE spectrum, a spectral peak in the frequency range comparable to Ω_H is, indeed, exactly at Ω_H. In the present section, we adopt this hypothesis in relation to the spectral peak labelled a in Fig. 2, and then follow its implications for the observed and simulated ICE spectra.

Let us first take the difference between the measured ICE power spectra before and during the burst event, in order to distinguish the spectral peaks that result from the burst event. This differenced ICE spectrum is plotted in Fig. 13, which can be considered as variant of Fig. 2. In Fig. 13, peak a appears at 32.73MHz, while the

three intense peaks b, c and d are at 252.3, 280.7 and 304.2MHz. Following the discussion in the preceding paragraph, the proton cyclotron frequency inferred from peak a is $\Omega_H = 32.73$MHz. This differs from the value $\Omega_H = 26.6$MHz used hitherto, which was estimated from the mean frequency separation of peaks b, c and d in Fig. 2. It implies a slightly different radial location, hence correspondingly different local plasma parameters which are used in our next set of simulations. The assumption that $\Omega_H = 32.73$MHz implies that the frequencies of the spectral peaks b, c and d correspond to $7.71\Omega_H$, $8.58\Omega_H$ and $9.29\ \Omega_H$ if they are excited at the same spatial location. This radial location is characterised by the local magnetic field strength $B \simeq 2.147$T, which for LHD outer edge implies $R = 4.234$m. At that position, the local plasma parameters including electron number density $n_e = 1.171 \times 10^{19}\mathrm{m}^{-3}$, thermal deuteron temperature $T_i = 2.4337$keV and electron temperature $T_e = 2.0466$keV.

Using these parameters, we have run multiple PIC-hybrid computations for 3.02MeV protons with values of $u_\perp/V_A$ in the range $[0.8, 1.3]$. As in sub-section 4.3, the corresponding parallel velocity $u_\parallel$ is obtained using Eq. 10. The spatial domain of our 1D3V computations is oriented such that there is an angle of 91.0° between $\mathbf{B}_0$ and all wavevectors $\mathbf{k}$. The relative number density of energetic protons at 3.02MeV compared to the thermal deuterons is $\xi = 0.001$ in our computations. Let us focus on the case $u_\perp/V_A = 1.2$. For fusion-born protons at their birth energy $E = 3.02$MeV, this implies $u_\parallel = \left[2E/m_H - (1.2V_A)^2\right]^{1/2} = 2.175V_A$.

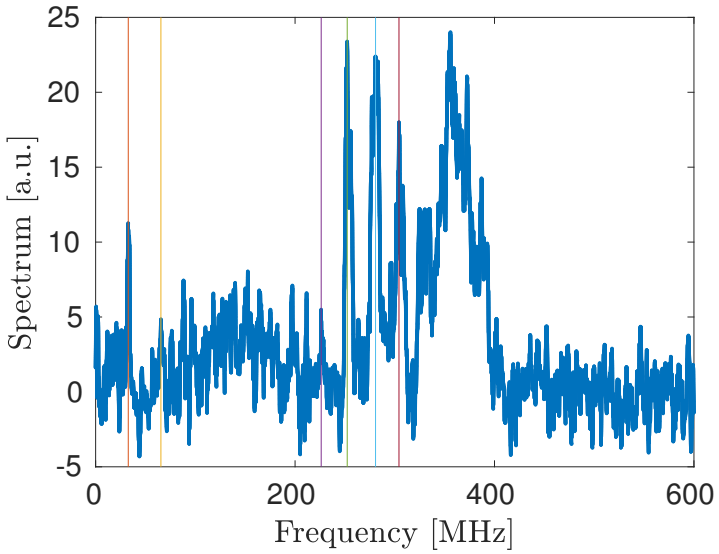

Figure 13: Difference between ICE spectra measured before and during the burst event in LHD plasma 133979, inferred from the dataset underlying Fig. 2. The vertical lines identify spectral peaks at 32.73MHz (red), 65.46MHz (yellow), 226.2MHz (purple), 252.3MHz (green), 280.7MHz (cyan), and 304.2MHz (dark red) MHz. These frequencies normalized to 32.73 MHz yield 1, 2, 6.911, 7.709, 8.576 and 9.294.

We therefore initialise the velocity distribution of energetic protons with parameter values $u_\perp = 1.2V_A$ and $u_\parallel = 2.175V_A$ in the representation $f_H\left(v_\perp, v_\parallel\right) = n_H/\left(2\pi v_\perp\right)\delta(v_\parallel - u_\parallel)\delta(v_\perp - u_\perp)$. The power spectrum of δB_z obtained from the corresponding PIC-hybrid computations is the green trace in Fig. 14. This displays shifted spectral peaks for the wave travelling forward, the strongest of which are at $7.64\Omega_H$, $8.57\Omega_H$ and $9.44\Omega_H$. These values are remarkably close to those peaks b, c and d in LHD in Fig. 2 which are at $7.71\Omega_H$, $8.58\Omega_H$ and $9.29\Omega_H$. In contrast, the PIC-hybrid simulated spectrum for an energetic proton population initialised with $u_\perp = 1.2V_A$ and $u_\parallel = 0$, plotted with a dark blue trace in Fig. 14, has dominant peaks at the exact cyclotron harmonics $7\Omega_H$, $8\Omega_H$ and $9\Omega_H$. This outcome suggests that the ICE burst is driven by 3.02MeV fusion-born protons with $u_\perp = 1.2V_A$ and $u_\parallel = 2.175V_A$. We emphasise that the frequency shift away from each integer cyclotron harmonic is not the same for all harmonics, and hence not simply Doppler in origin: both in the observations, and in our simulations. First principles PIC-hybrid simulations, extending into the nonlinear regime of the MCI, are essential in recovering the frequency shifts.

An additional feature of interest in Fig. 14 is the relative strength of the peak at the fundamental Ω_H, which is more pronounced than neighbouring harmonics. The lower harmonics up to $\ell \approx 6$ are linearly stable in our PIC-hybrid computations, and are driven later, in the nonlinear stage. This is shown in Fig. 15. This aspect of MCI physics was discussed in Cook et al. [28], Carbajal et al. [21] and

$u_\perp$, $u_\parallel$ \ ℓ	5	6	7	8	9
$u_\perp = 1.100V_A$, $u_\parallel = 2.228V_A$	5.769	6.769	7.703	8.570	9.57
$u_\perp = 1.200V_A$, $u_\parallel = 2.175V_A$	5.835	6.702	7.636	8.570	9.436
$u_\perp = 1.250V_A$, $u_\parallel = 2.147V_A$	5.769	6.702	7.636	8.570	9.436
$u_\perp = 1.300V_A$, $u_\parallel = 2.117V_A$	5.769	6.702	7.636	8.570	9.436

Table 5: Spectral peak frequencies in units of Ω_H, for four PIC-hybrid computations appropriate to the location where $\Omega_H = 32.73$MHz in LHD. The integer values of ℓ, labelling columns, denote the cyclotron harmonic for the $u_\parallel = 0$ case, from which the spectral peaks has shifted. These results correspond to waves propagating at an angle of 91° with respect to the background magnetic field $\mathbf{B}_0$.

Chapman et al. [24, 25].

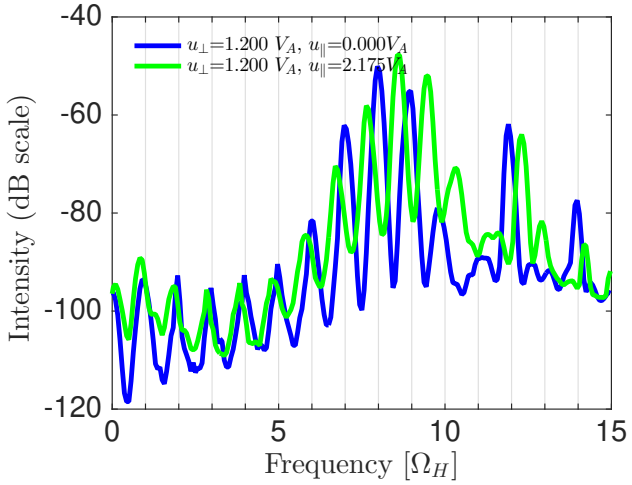

Figure 14: Simulated ICE power spectra obtained from two PIC-hybrid computations for the case $\Omega_H = 32.73$MHz with $u_\perp/V_A = 1.2$: blue trace, $u_\parallel = 0$, green trace, $u_\parallel = 2.175V_A$. These parameters determine the initial velocity distribution of the energetic minority proton population, which is represented by $n_H/(2\pi v_\perp)\delta(v_\parallel)\delta(v_\perp - u_\perp)$. For the green trace, these velocity parameters take the dimensional values $u_\parallel = 2.106 \times 10^7 \mathrm{ms}^{-1}$ and $u_\perp = 1.161 \times 10^7 \mathrm{ms}^{-1}$ and are such that $1/2m_H(u_\parallel^2 + u_\perp^2) = 3.02$MeV, which is the birth enery of fusion-born protons in deuterium plasma. The blue trace spectral peaks are at integer proton cyclotron harmonics. In contrast, the three dominant spectral peaks in the green trace are at $7.64\Omega_H$, $8.57\Omega_H$ and $9.44\Omega_H$. The corresponding experimental ICE spectral peaks from LHD are (see Fig. 13) at $7.71\Omega_H$, $8.58\Omega_H$, and $9.29\Omega_H$. The simulation domain is oriented at 91° to the background magnetic field.

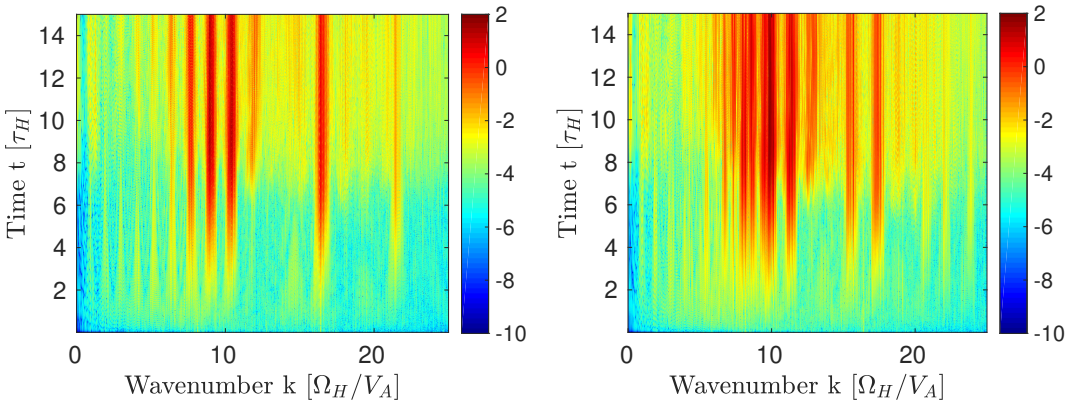

Figure 15: Time evolution of the power density of the spatial fast Fourier transform of δB_z, as a function of normalised wavenumber Ω_H/V_A, shown on a $\log_{10}$ scale. This shows how the distribution of spectral power across proton cyclotron harmonic frequency range changes with time in our PIC-hybrid computations. In both panels, the energetic proton minority population is initialised with $u_\perp = 1.2V_A$: left panel, $u_\parallel = 0$; right panel $u_\parallel = 2.175$. The blue (green) traces in Fig. 14 correspond to time-integrated versions of the left (right) panels here. The intensity at the fundamental cyclotron frequency increases in the later stage of the simulations, $t \geq 8\tau_D$.

6 Conclusions

We have obtained power spectra for the fluctuating part of the magnetic field δB_z from multiple PIC-hybrid computations of the collisionless relaxation of a fresh fusion-born proton population. All the simulated ICE spectra show dominant spectral peaks separated approximately by the cyclotron harmonic frequency Ω_H, in the frequency range between $8\Omega_H$ and $12\Omega_H$, see section 4 ($7\Omega_H$ and $11\Omega_H$, see section 5). Our approach attempts to account for all these peaks at once, in which case one would favor the origin of ICE at 4.234m. In contrast, the newly termed ICE "chemistry" does not rule out that peak a could originate from a different location as compared with the emission location of peaks b, c and d. The observed peak frequencies are shifted by a significant fraction of Ω_H relative to integer values. We find good mappings from the simulated spectra to the three intense peaks from the measured LHD spectrum in Fig. 2, provided that the protons are initialised with $v_\parallel \approx 2.5V_A$, consistent with $v_\perp \approx V_A$ and $E_p = 3.02$MeV. The simulated spectra result from the collisionless relaxation of these protons via the magnetoacoustic cyclotron instability for parameters relevant to a bursting ICE event during LHD deuterium plasma 133979. This excites waves that propagate almost perpendicular to the background magnetic field. The simulated results have been obtained using a simple drifting ring, and additional simulations show that the inclusion of thermal spread in the ring only slightly affects the relative strength of the most intense harmonics. The propagation angle also affects the

calculated spectra. Having noted these relatively minor sensitivities, the underlying conclusion appears robust: the measured ICE spectrum from LHD deuterium plasma 133979 shown in Fig. 2 is probably excited by the fast relaxation of a transient local population of fusion-born protons at 3.02MeV whose perpendicular velocity is close to the Alfvén speed, and whose parallel velocity is therefore $\sim$ 2.5 times higher. We believe this may be the first observation of collective radiation from a confined population of fusion born-ions to be reported from a heliotron-stellarator plasma.

7 Acknowledgments

This work has been carried out within the framework of the EUROfusion Consortium and has received funding from the Euratom research and training programme 2014-2018 and 2019-2020 under grant agreement No 633053. The work received support from the RCUK Energy Programme [grant number EP/T012250/1], NIFS budget NIFS15KLPF045 and from NRF Korea grant no. 2014M1A7A1A03029881. The views and opinions expressed herein do not necessarily reflect those of the European Commission. ROD acknowledges the hospitality of Kyushu University. BCGR acknowledges helpful discussions with Prof. M. Koepke and with Dr. Carbajal-Gomez.

References

[1] Y Takeiri, T Morisaki, M Osakabe, M Yokoyama, S Sakakibara, H Takahashi, Y Nakamura, T Oishi, G Motojima, S Murakami, et al. Extension of the operational regime of the lhd towards a deuterium experiment. *Nuclear Fusion*, 57(10):102023, 2017.

[2] M Osakabe, Y Takeiri, T Morisaki, G Motojima, K Ogawa, M Isobe, M Tanaka, S Murakami, A Shimizu, K Nagaoka, et al. Current status of large helical device and its prospect for deuterium experiment. *Fusion Science and Technology*, 72(3):199–210, 2017.

[3] Yasuhiko Takeiri. The large helical device: entering deuterium experiment phase toward steady-state helical fusion reactor based on achievements in hydrogen experiment phase. *IEEE Transactions on Plasma Science*, 46(7): 2348–2353, 2018.

[4] Masaki Osakabe, Mitsutaka Isobe, Masahiro Tanaka, Gen Motojima, Katsuyoshi Tsumori, Masayuki Yokoyama, Tomohiro Morisaki, and Yasuhiko Takeiri. Preparation and commissioning for the lhd deuterium experiment. *IEEE Transactions on Plasma Science*, 46(6):2324–2331, 2018.

[5] Makoto Kobayashi, Tomoyo Tanaka, Takeo Nishitani, Kunihiro Ogawa, Mitsutaka Isobe, Akemi Kato, Takuya Saze, Sachiko Yoshihashi, Masaki Osak-

abe, LHD Experiment Group, et al. First measurements of thermal neutron distribution in the lhd torus hall generated by deuterium experiments. *Fusion Engineering and Design*, 137:191–195, 2018.

[6] M Isobe, K Ogawa, T Nishitani, N Pu, H Kawase, R Seki, H Nuga, E Takada, S Murakami, Y Suzuki, et al. Fusion neutron production with deuterium neutral beam injection and enhancement of energetic-particle physics study in the large helical device. *Nuclear Fusion*, 58(8):082004, 2018.

[7] Tomoyo Tanaka, Sachiko Yoshihashi, Makoto Kobayashi, Akira Uritani, Kenichi Watanabe, Atsushi Yamazaki, Takeo Nishitani, Kunihiro Ogawa, and Mitsutaka Isobe. Measurement of neutron spectrum using activation method in deuterium plasma experiment at lhd. *Fusion Engineering and Design*, 2019.

[8] CM Muscatello, WW Heidbrink, RL Boivin, C Chrystal, CS Collins, Y Fujiwara, and H Yamaguchi. Diagnosis of fast ions produced by negative-ion neutral-beam injection with fast-ion deuterium-alpha spectroscopy. *Review of Scientific Instruments*, 90(7):073504, 2019.

[9] G.A. Cottrell, V.P. Bhatnagar, O. Da Costa, R.O. Dendy, J. Jacquinot, K.G. McClements, D.C. McCune, M.F.F. Nave, P. Smeulders, and D.F.H. Start. Ion cyclotron emission measurements during JET deuterium-tritium experi-

ments. *Nuclear Fusion*, 33(9):1365, 1993. doi: 10.1088/0029-5515/33/9/I10. URL http://iopscience.iop.org/0029-5515/33/9/I10/.

[10] Richard Dendy, Ben Chapman, Bernard Reman, Sandra Chapman, Tsuyoshi Akiyama, and Gunsu Yun. Modelling ion cyclotron emission from kstar tokamak and lhd helical device plasmas. In *APS Meeting Abstracts*, 2017.

[11] XD Du, K Toi, M Osakabe, S Ohdachi, T Ido, K Tanaka, M Yokoyama, M Yoshinuma, K Ogawa, KY Watanabe, et al. Resistive interchange modes destabilized by helically trapped energetic ions in a helical plasma. *Physical review letters*, 114(15):155003, 2015.

[12] XD Du, K Toi, S Ohdachi, M Osakabe, T Ido, K Tanaka, M Yokoyama, M Yoshinuma, K Ogawa, KY Watanabe, et al. Resistive interchange mode destabilized by helically trapped energetic ions and its effects on energetic ions and bulk plasma in a helical plasma. *Nuclear Fusion*, 56(1):016002, 2015.

[13] CA Michael, K Tanaka, T Akiyama, T Ozaki, M Osakabe, Satoru Sakakibara, H Yamaguchi, S Murakami, M Yokoyama, M Shoji, et al. Role of helium–hydrogen ratio on energetic interchange mode behaviour and its effect on ion temperature and micro-turbulence in lhd. *Nuclear Fusion*, 58(4):046013, 2018.

[14] S Ohdachi, T Bando, K Nagaoka, H Takahashi, Y Suzuki, KY Watanabe, XD Du, K Toi, M Osakabe, and T Morisaki. Excitation mechanism of the energetic particle driven resistive interchange mode and strategy to control the mode in large helical device. In *27th IAEA Fusion Energy Conference, Gandhinagar, India*, pages 22–27, 2018.

[15] T Bando, S Ohdachi, M Isobe, Y Suzuki, K Toi, K Nagaoka, H Takahashi, R Seki, XD Du, K Ogawa, et al. Excitation of helically-trapped-energetic-ion driven resistive interchange modes with intense deuterium beam injection and enhanced effect on beam ions/bulk plasmas of lhd. *Nuclear Fusion*, 58 (8):082025, 2018.

[16] K Ida, T Kobayashi, K Itoh, M Yoshinuma, T Tokuzawa, T Akiyama, C Moon, H Tsuchiya, S Inagaki, and S-I Itoh. Abrupt onset of tongue deformation and phase space response of ions in magnetically-confined plasmas. *Scientific Reports*, 6:36217, 2016.

[17] K Ida, T Kobayashi, M Yoshinuma, T Akiyama, T Tokuzawa, H Tsuchiya, K Itoh, and LHD Experiment Group. Observation of distorted maxwell-boltzmann distribution of epithermal ions in lhd. *Physics of Plasmas*, 24 (12):122502, 2017.

[18] Shoichi Sato, Makoto Ichimura, Yuusuke Yamaguchi, Makoto Katano, Yasutaka Imai, Tatsuya Murakami, Yuichiro Miyake, Takuro Yokoyama, Shinichi

Moriyama, Takayuki Kobayashi, et al. Observation of ion cyclotron emission owing to DD fusion product H ions in JT-60U. *Plasma and Fusion Research*, 5:S2067–S2067, 2010.

[19] D. Winske and N. Omidi. Hybrid codes: Methods and applications. Technical report, Los Alamos National Lab., NM (USA), 1991.

[20] Winske, Dan, Yin, Lin, Omidi, Nick, Karimabadi, Homa, Quest, and Kevin. Hybrid simulation codes: Past, present and future A tutorial. pages 136–165, 2003.

[21] L. Carbajal, R. O. Dendy, S.C. Chapman, and J.W.S. Cook. Linear and nonlinear physics of the magnetoacoustic cyclotron instability of fusion born-ions in relation to ion cyclotron emission. *Physics of Plasmas*, 21(1):012106, 2014.

[22] L. Carbajal, R.O. Dendy, S.C. Chapman, and J.W.S. Cook. Quantifying fusion born ion populations in magnetically confined plasmas using ion cyclotron emission. *Physical Review Letters*, 118(10):105001, 2017.

[23] Bernard CG Reman, Richard Dendy, Tsuyoshi Akiyama, Sandra C Chapman, James WS Cook, Hiroe Igami, Shigeru Inagaki, Kenji Saito, and Gunsu S Yun. Interpreting observations of ion cyclotron emission from large helical device plasmas with beam-injected ion populations. *Nuclear Fusion*, 2019.

[24] B. Chapman, R.O. Dendy, K.G. McClements, S.C. Chapman, G.S. Yun, S.G. Thatipamula, and M.H. Kim. Sub-microsecond temporal evolution of edge density during edge localized modes in KSTAR tokamak plasmas inferred from ion cyclotron emission. *Nuclear Fusion*, 57(12):124004, 2017.

[25] Benjamin Chapman, Richard O. Dendy, Sandra C. Chapman, Kenneth G. McClements, Gunsu S. Yun, Shekar Goud Thatipamula, and Minho Kim. Nonlinear wave interactions generate high-harmonic cyclotron emission from fusion-born protons during a KSTAR ELM crash. *Nuclear Fusion*, 58(9): 096027, 2018.

[26] B Chapman, RO Dendy, SC Chapman, KG McClements, GS Yun, SG Thatipamula, and MH Kim. Interpretation of suprathermal emission at deuteron cyclotron harmonics from deuterium plasmas heated by neutral beam injection in the kstar tokamak. *Nuclear Fusion*, 59(10):106021, 2019.

[27] R.O. Dendy, K.G. McClements, C.N. Lashmore-Davies, G.A. Cottrell, R. Majeski, and S. Cauffman. Ion cyclotron emission due to collective instability of fusion products and beam ions in TFTR and JET. *Nuclear Fusion*, 35(12): 1733, 1995.

[28] J.W.S. Cook, R. O. Dendy, and S.C. Chapman. Particle-in-cell simulations of the magnetoacoustic cyclotron instability of fusion-born alpha particles

in tokamak plasmas. *Plasma Physics and Controlled Fusion*, 55(6):065003, 2013.

[29] J.W.S. Cook, R.O. Dendy, and S.C. Chapman. Stimulated emission of fast Alfvén waves within magnetically confined fusion plasmas. *Physical Review Letters*, 118(18):185001, 2017.

[30] V.S. Belikov and Ya. I. Kolesnichenko. *Soviet Physics Technical Physics*, 20: 1146, 1976.

[31] R.O. Dendy, Chris N. Lashmore Davies, and K.F. Kam. A possible excitation mechanism for observed superthermal ion cyclotron emission from tokamak plasmas. *Physics of Fluids B: Plasma Physics (1989-1993)*, 4(12):3996–4006, 1992. doi: 10.1063/1.860304. URL http://scitation.aip.org/content/aip/journal/pofb/4/12/10.1063/1.860304.

[32] R. O. Dendy, C.N. Lashmore Davies, and K. F. Kam. The magnetoacoustic cyclotron instability of an extended shell distribution of energetic ions. *Physics of Fluids B: Plasma Physics (1989-1993)*, 5(7):1937–1944, 1993.

[33] S. Cauffman, R. Majeski, K.G. McClements, and R.O. Dendy. Alfvénic behaviour of alpha particle driven ion cyclotron emission in TFTR. *Nuclear Fusion*, 35(12):1597, 1995.

[34] Yutaka Matsumoto, Tatsuhiko Nagaura, Shun-ichi Oikawa, and Tsuguhiro

Watanabe. Particle orbit analysis under the ion cyclotron range of frequency heating in the large helical device. *Japanese journal of applied physics*, 43 (1R):332, 2004.

[35] Ryousuke Seki, Yutaka Matsumoto, Yasuhiro Suzuki, Kiyomasa Watanabe, and Masafumi Itagaki. Particle orbit analysis in the finite beta plasma of the large helical device using real coordinates. *Plasma and Fusion Research*, 3: 016–016, 2008.

[36] Dmitry Moseev and Mirko Salewski. Bi-maxwellian, slowing-down, and ring velocity distributions of fast ions in magnetized plasmas. *Physics of Plasmas*, 26(2):020901, 2019.

[37] R.O. Dendy, C.N. Lashmore-Davies, K.G. McClements, and G.A. Cottrell. The excitation of obliquely propagating fast Alfvén waves at fusion ion cyclotron harmonics. *Physics of plasmas*, 1(6):1918–1928, 1994. doi: 10.1063/1.870647. URL http://dx.doi.org/10.1063/1.870647.

[38] S. Cauffman, R. Majeski, K. G. McClements, and R. O. Dendy. Alfvenic behaviour of alpha particle driven ion cyclotron emission in TFTR. *Nuclear Fusion*, 35:1597–1602, 1995. URL http://iopscience.iop.org/0029-5515/35/12/I22.

[39] S. Cauffman and R. Majeski. Ion cyclotron emission on the Tokamak Fusion Fest Reactor. *Review of Scientific Instruments*, 66(1):817–819, 1995.

[40] K.G. McClements, C. Hunt, R.O. Dendy, and G.A. Cottrell. Ion cyclotron emission from JET DT plasmas. *Physical review letters*, 82(10):2099–2102, 1999. URL http://0-journals.aps.org.pugwash.lib.warwick.ac.uk/prl/pdf/10.1103/PhysRevLett.82.2099.

[41] R. O. Dendy and K.G. McClements. Ion cyclotron emission from fusion-born ions in large tokamak plasmas: a brief review from JET and TFTR to ITER. *Plasma Phys. Control. Fusion*, 57(4):044002, 2015.

[42] R Ochoukov, V Bobkov, B Chapman, R Dendy, M Dunne, H Faugel, M García-Muñoz, B Geiger, P Hennequin, KG McClements, et al. Observations of core ion cyclotron emission on asdex upgrade tokamak. *Review of Scientific Instruments*, 89(10):10J101, 2018.

[43] Kathreen E Thome, David C Pace, Robert I Pinsker, Michael A Van Zeeland, William W Heidbrink, and Max E Austin. Central ion cyclotron emission in the diii-d tokamak. *Nuclear Fusion*, 2019.

[44] R Ochoukov, R Bilato, V Bobkov, B Chapman, SC Chapman, RO Dendy, M Dunne, H Faugel, M García-Muñoz, B Geiger, et al. Core plasma ion cyclotron emission driven by fusion-born ions. *Nuclear Fusion*, 59(1):014001, 2018.

[45] Roman Ochoukov, Kenneth G McClements, Roberto Bilato, Volodymyr V Bobkov, Benjamin Chapman, Sandra C Chapman, Richard Dendy, Mykola

Dreval, Helmut Faugel, Jean-Marie Noterdaeme, et al. Interpretation of core ion cyclotron emission driven by sub-alfvénic beam-injected ions via magnetoacoustic cyclotron instability. *Nuclear Fusion*, 2019.

[46] Kenji Saito, Hiroe Igami, Mieko Toida, Tsuyoshi Akiyama, Shuji Kamio, Ryosuke Seki, LHD Experiment Group, et al. Rf wave detection with high-frequency magnetic probes in lhd. *Plasma and Fusion Research*, 13:3402043–3402043, 2018.

[47] M. Ichimura, M. Katano, Y. Yamaguchi, S. Sato, Y. Motegi, H. Muro, T. Ouchi, S. Moriyama, M. Ishikawa, K. Shinohara, et al. Study of ion cyclotron emissions due to DD fusion product ions on JT-60U. Technical report, Geneva, 2008.

[48] M. Ichimura, H. Higaki, S. Kakimoto, Y. Yamaguchi, K. Nemoto, M. Katano, M. Ishikawa, S. Moriyama, and T. Suzuki. Observation of spontaneously excited waves in the ion cyclotron frequency range on JT-60U. *Nuclear Fusion*, 48(3):035012, 2008. doi: 10.1088/0029-5515/48/3/035012. URL http://dx.doi.org/10.1088/0029-5515/48/3/035012.

[49] Mirko Salewski, Benedikt Geiger, Asger Schou Jacobsen, M García-Muñoz, WW Heidbrink, Søren Bang Korsholm, Frank Leipold, Jens Madsen, Dmitry Moseev, Stefan Kragh Nielsen, et al. Measurement of a 2d fast-ion velocity

distribution function by tomographic inversion of fast-ion d-alpha spectra. *Nuclear fusion*, 54(2):023005, 2014.

[50] Dmitry Moseev, Mirko Salewski, M Garcia-Muñoz, B Geiger, and M Nocente. Recent progress in fast-ion diagnostics for magnetically confined plasmas. *Reviews of Modern Plasma Physics*, 2(1):7, 2018.

[51] Mirko Salewski, M Nocente, Birgitte Madsen, I Abramovic, G Gorini, AS Jacobsen, VG Kiptily, Søren Bang Korsholm, Dmitry Moseev, Stefan Kragh Nielsen, et al. Diagnostic of fast-ion energy spectra and densities in magnetized plasmas. *Journal of Instrumentation*, 14(05):C05019, 2019.

[52] G Yun and T Akiyama. Fast rf spectrometer system on lhd. *Annual Report of National Institute for Fusion Science*, 2012:46, .

[53] G Yun and T Akiyama. Fast rf spectrometer system on lhd. *Annual Report of National Institute for Fusion Science*, 2013:53, .

[54] G Yun and T Akiyama. Fast rf spectrometer system on lhd. *Annual Report of National Institute for Fusion Science*, 2014:58, .

[55] T Mutoh, R Kumazawa, T Seki, K Saito, H Kasahara, Y Nakamura, S Masuzaki, S Kubo, Y Takeiri, T Shimozuma, et al. Steady-state operation and high energy particle production of mev energy in the large helical device. *Nuclear Fusion*, 47(9):1250, 2007.

[56] Tsuguhiro Watanabe, Junichi Miyazawa, Hiroshi Yamada, Sadayoshi Murakami, Suguru Masuzaki, Masaki Osakabe, Mitsutaka Isobe, Masayuki Tokitani, and Osamu Motojima. Discriminating acquisition of 15-mev protons from d-3he fusion reaction in lhd. *Plasma and Fusion Research*, 3:058–058, 2008.

[57] R.O. Dendy, K.G. McClements, C.N. Lashmore-Davies, R. Majeski, and S. Cauffman. A mechanism for beam-driven excitation of ion cyclotron harmonic waves in the Tokamak Fusion Test Reactor. *Physics of Plasmas*, 1 (10):3407–3413, 1994.

[58] Tünde Fülöp and Mietek Lisak. Ion cyclotron emission from fusion products and beam ions in the Tokamak Fusion Test Reactor. *Nuclear Fusion*, 38(5): 761, 1998.